Volume 6
Number 12
December 2025
Pages 1825–1952

RSC Chemical Biology

rsc.li/rsc-chembio

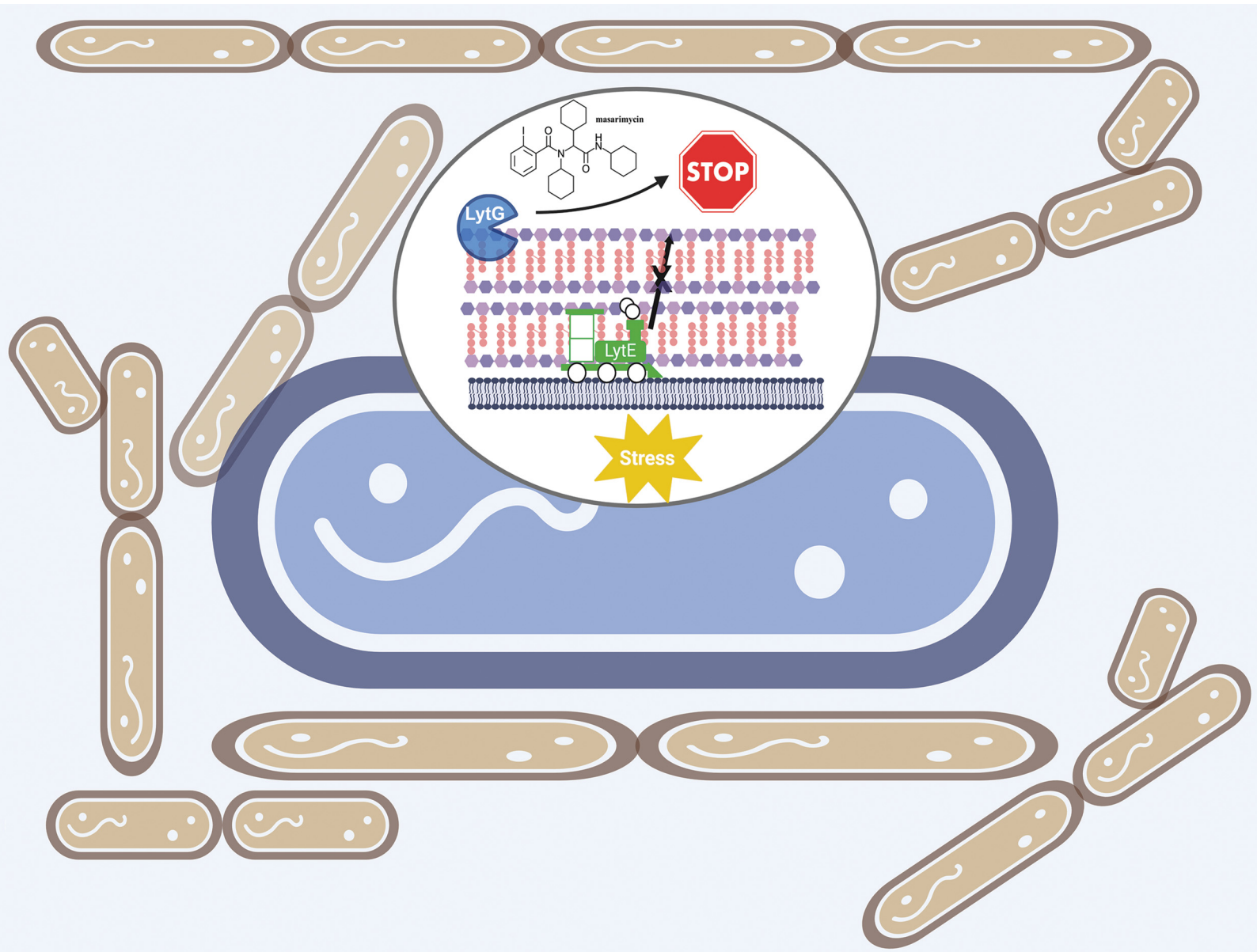

ISSN 2633-0679

ROYAL SOCIETY OF CHEMISTRY

PAPER

Christopher W. Reid *et al.*
A Lyt at the end of the tunnel? Unraveling the complex interactions of the *N*-acetylglucosaminidase LytG in cell wall metabolism

RSC Chemical Biology

ROYAL SOCIETY OF CHEMISTRY

PAPER

View Article Online
View Journal | View Issue

Cite this: *RSC Chem. Biol.*, 2025, **6**, 1848

A Lyt at the end of the tunnel? Unraveling the complex interactions of the *N*-acetylglucosaminidase LytG in cell wall metabolism

Jazmeen Hernandez,[a] Jett Duval,[a] Taryn Rauff,[a] Ethan Hall,[a] Mika Gallati,[a] Brad A. Haubrich,[b] Monica Thoma,[a] Elimelec Aponte,[a] Amit Basu,[c] Joseph A. DeGiorgis[de] and Christopher W. Reid *[af]

Received 11th June 2025,
Accepted 25th September 2025

DOI: 10.1039/d5cb00151j

rsc.li/rsc-chembio

The growth and division of the Gram-positive cell requires the coordinated action of enzymes involved in the synthesis and degradation of the heteropolymer peptidoglycan. Herein, we present the use of the diamide masarimycin, an inhibitor of the *exo*-*N*-acetylglucosaminidase (GlcNAcase) LytG from *Bacillus subtilis*, as a chemical biology probe to elucidate the biological role of this cell wall degrading enzyme. Using a combination of chemical biology and genetic approaches we provide the first evidence that LytG activity influences the elongation and division complexes in *B. subtilis*. Chemical inhibition of LytG resulted in dysregulated cell elongation and localization of the division plane and the induction of the cell wall stress response. In the presence of masarimycin, cells show asymmetrical thickening of the cell wall and dysregulation of division plane localization. The use of genetic and synergy/antagonism screens established connections to late-stage peptidoglycan synthesis, particularly related to cross-linking function. These results stand in stark contrast to those observed for the Δ*lytG* knockout, which does not exhibit these phenotypes. Cell-wall labelling with a fluorescent D-amino acid and muropeptide analysis has highlighted a functional connection between LytG, the carboxypeptidase DacA, and D,D-endopeptidases. These results highlight the use of chemical probes such as masarimycin to inform on the biological function of autolysins by providing insight into the role LytG plays in cell growth and division.

Introduction

Bacillus subtilis is a fast-growing, aerobic, rod-shaped bacterium and is one of the best studied Gram-positive organisms.[1] The cell shape of most bacteria is maintained by the cell wall, which protects the cell from the outward facing turgor pressure.[2] The cell wall of *B. subtilis* contains two major cell wall components, the heteropolymer peptidoglycan (PG) and the anionic polymers wall-teichoic acid (WTA) and lipoteichoic acid (LTA).[3] PG is composed of alternating *N*-acetylglucosamine (GlcNAc) and *N*-acetylmuramic acid (MurNAc) residues linked by a β-(1 → 4) glycosidic linkage (Fig. 1). Adjacent polysaccharide strands are cross-linked *via* stem peptides attached to the C-3 lactyl moiety of MurNAc to form a three-dimensional mesh.[2] The current model of PG synthesis in Gram-positive organisms invokes the 'essential' degrading enzymes for the incorporation of nascent PG into the stress bearing layer.[4–6] In this model, controlled degradation of PG is required for cell maintenance, elongation, and division, and this tightly regulated process is suggested to involve the interplay between synthetic and degradative enzymes.[4,7,8] Bacterial autolysins are a highly diverse group of enzymes capable of cleaving bonds in polymeric PG, and participate in cell wall growth and its regulation.[9] The degradative enzymes fall into 4 broad classes based on their activity: lytic transglycosylases, *N*-acetylglucosaminidases (GlcNAcases) and muramidases, L-alanine amidases, and endopeptidases. Deciphering the physiological role of autolysins has been a formidable task as functional redundancy complicates

[a] *Department of Biological and Biomedical Sciences, Bryant University, 1150 Douglas Pike, Smithfield, RI 02917, USA. E-mail: creid@bryant.edu*
[b] *Department of Basic Sciences College of Osteopathic Medicine, Touro University, Nevada Henderson, NV, 89014, USA*
[c] *Department of Chemistry, Brown University, 324 Brook Street, Providence, RI 02912, USA*
[d] *Department of Biology Providence College 1 Cunningham Square, Providence, RI 02918, USA*
[e] *Whitman Center Marine Biological Laboratory, 7 Water St. Woods, Hole, MA 02543, USA*
[f] *Center for Health and Behavioral Sciences Bryant University, 1150 Douglas Pike, Smithfield, RI, 02917, USA*

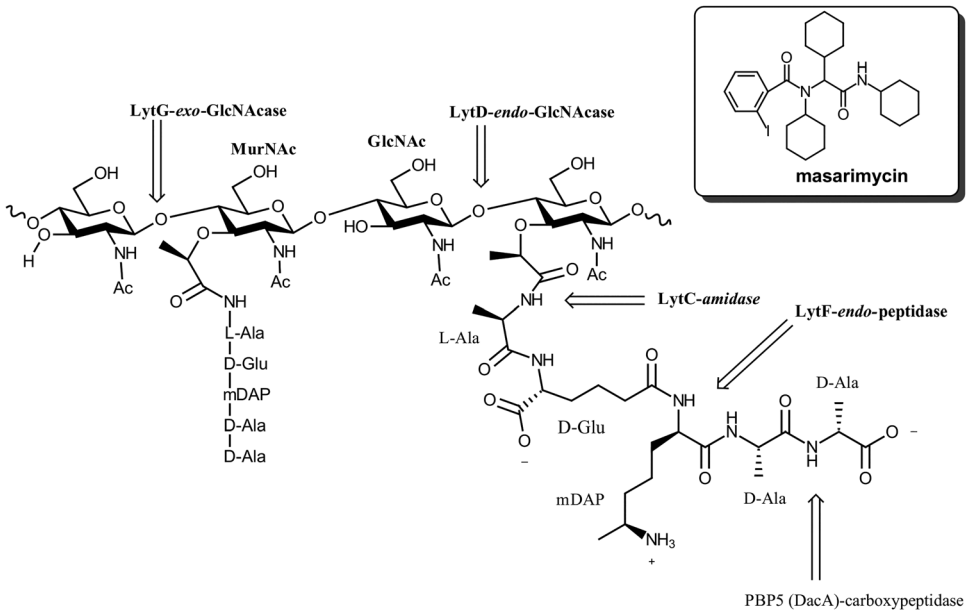

Fig. 1 Structure of peptidoglycan showing the cleavage sites of the major autolysins in *Bacillus subtilis*. Inset, structure of Mas, an inhibitor of the *exo*-acting GlcNAcase LytG.

attribution of biological activity.[10] Recent biophysical[4,11] and computational studies[12] of bacterial autolysins have begun to unravel their roles in the release of stress in the cell wall to allow for incorporation of new material. A renaissance in PG metabolism research has started to provide new chemical biology tools to study synthesis.[13–17] While the cell wall, and PG in particular, have provided a wealth of clinically relevant antimicrobial targets,[7] our understanding of the complex interplay between degradative and synthetic steps is still underdeveloped.

We have previously demonstrated the utility of glycosyl triazoles[18] and diamides[19,20] as a scaffold for developing inhibitors of bacterial cell wall hydrolases, in particular GlcNAcases in *B. subtilis* and *Streptococcus pneumoniae*.[20] To our knowledge these are the first inhibitors of autolysins that also inhibit cell growth. These probes can be used to interrogate Gram-positive cell wall metabolism in a manner orthogonal to traditional genetic approaches. Here we report on the application of the bacteriostatic inhibitor of LytG, masarimycin (Mas)[19,20] to interrogate cell wall metabolism in *B. subtilis*. LytG is the major active GlcNAcase during vegetative growth[21] yet its exact role has remained elusive. Mas (Fig. 1, inset) was identified as a bacteriostatic inhibitor of *B. subtilis* growth with an MIC of 4 μM. *B. subtilis* grown in the presence of Mas exhibited a morphological phenotype akin to sausage links, with strings of cells linked together without separating completely. In an *in vitro* assay of LytG activity, Mas exhibited an IC_{50} of 48 μM. These initial studies also indicated that Mas exhibted increased potency against strains of *B. subtilis* lacking the autolysins LytC, LytD, or LytF.[19] This was a puzzling result, but suggested a complex interplay between autolysin activity, and highlighted the need for additional studies to evaluate the role of Mas and LytG in bacterial cell wall processing. In this paper, we now report on the ability of Mas to inform on biological function when used in tandem with genetic and molecular approaches. Our results provide fresh insight into the role LytG plays in cell growth and division.

Methods

Bacterial strains and growth conditions

B. subtilis strains used in this study can be found in Table S1. All strains were grown in Lauria-Bertani broth (LB) or agar plates supplemented with the appropriate antibiotics at 37 °C. When appropriate erythromycin or kanamycin was incorporated at a concentration of 1 μg mL^{-1}.

Preparation of masarimycin

Masarimycin was prepared as previously described using microwave-assisted organic synthesis.[22] Material showed single product by TLC and NMR (SI).

Minimum inhibitory concentration (MIC) assay

MIC values were determined using the resazurin method.[22,23] Briefly, cells were initially grown from the freezer on LB plates. For all assays second passage cells of *B. subtilis* 11774, 3610, and associated knockout strains (Table S1) were used and grown overnight in LB broth, and standardized to an OD_{600nm} = 1.0. For masarimycin, serial dilutions were initially made in DMSO down to a concentration of 100 μM, further dilutions were then made into PBS. Plates containing LB broth were inoculated with a 1/20 dilution of the OD_{600nm} = 1.0 cell culture with a final concentration of no more than 1% DMSO. Cultures were grown statically under aerobic conditions for 4 h at 37 °C, followed by addition of 30 μL of a 0.01% (m/v) solution

of resazurin. The plates were incubated for 15 min to allow stabilization of color production. MICs were read directly off the plate; MICs were recorded as the lowest concentration that completely inhibited growth (purple).

Synergy and antagonism assays and fractional inhibitory concentration index calculation

Fractional inhibitory concentration index (FIC_{Index}) was conducted to determine the interaction between masarimycin and a range of antibiotics with defined mode-of-action or cell wall precursors in a 96 well-plate microdilution broth assay. A checkerboard assay was performed with each masarimycin pair as previously described.[24] Plates were inoculated with 5 μL of a OD_{600nm} = 1.0 culture of *B. subtilis* and growth monitored as previously described for the MIC assays. FIC_{Index} was determined using the formulae:

$$FIC = \frac{X}{MIC_x}, \quad (1)$$

where X is the lowest inhibitory concentration of the drug in the presence of the co-drug, and MIC_x is the lowest inhibitory concentration of the drug in the absence of the co-drug.

$$FIC_{Index} = FIC_{masarimycin} + FIC_{antibiotic} \quad (2)$$

Drug interactions were rated as synergistic ($FIC_{Index} \leq 0.5$), additive ($0.5 < FIC_{Index} \leq 1.0$), indifferent ($1.0 < FIC_{Index} \leq 4.0$), and antagonistic ($FIC_{Index} > 4.0$), based on published standards.[25]

Gene expression analysis

B. subtilis 11774 was grown to OD_{600nm} = 0.2 in LB broth at 37 °C with shaking and inoculated with either 3× MIC Mas (12 μM), cefoxitin (3 μM), or vehicle control DMSO (0.1% v/v) and incubated for 20 min. Cells were harvested (8000 rpm, 15 min, 4 °C) and total RNA extracted using Purezol (BioRad) following manufacturer's directions. Contaminating gDNA was removed and cDNA synthesized using iScript gDNA clear and cDNA synthesis kit (BioRad) and total cDNA quantified using Qubit ssDNA assay (Invitrogen). All qPCR assays were performed on a BioRad CFX96 Real Time System (BioRad) using hard-shell thin-wall 96-well plates closed with optically clear adhesive film. The reactions were performed in a final volume of 25 μL using a serial dilution of the appropriate template cDNA (2 μL) and using the iTaq Universal SYBR green supermix (BioRad). Amplification of target *relA* was performed with primers RelA-a 5′-TGA GCA TCT TCA GCG TAC AG-3′ and RelA-s 5′-TGA CTG CCG AGC AAG TTA TAG-3′. Transcript levels were normalized to the housekeeping gene 16srDNA using previously published primers 341F 5′-CCTACGGGAGGCAGC AG-3′ and 534R (5′-ATTACCGCGGCTGCTTGG-3′).[26] No Template (NTC) and no reverse-transcriptase (NRT) controls were included in each assay using DNase and RNase free water. The PCR cycle used was 95 °C, 3.00 min|95.0 °C, 10 s; 55 °C, 30 s; (39×)|25 °C, 5 s; ramp to 95 °C at 1 °C min^{-1}. All experiments were performed in biological and technical duplicate. Results were analyzed using BioRad CMX manager and GrapPad Prism software.

Isolation of peptidoglycan

Peptidoglycan was isolated following the procedure described by Schuab and Dillard.[27] Briefly, second passage cells of *B. subtilis* were grown in 50 mL LB to an OD_{600nm} = 0.2. Cells were treated with 0.75× MIC of Mas (MIC 4 μM) or an equivalent volume of DMSO (vehicle control) and incubated for 2 hours at 37 °C with shaking. Cells were harvested (9000× rpm, 15 min, 4 °C). The cell pellets were resuspended in 25 mM NaH_2PO_4 pH 6.0 containing 4% SDS and boiled for 30 min. Samples were allowed to cool to room temperature and centrifuged (15 000× rpm, 20 min) to pellet the SDS-insoluble (cell wall) material. The pellet was washed repeatedly with 25 mM NaH_2PO_4 pH 6.0 and centrifuged (15 000 rpm, 20 min) to remove the SDS. Wall teichoic acids were removed with 1 M HCl for 4 h at 37 °C with shaking followed by neutralization to pH 6 (litmus paper) and cell wall material isolated by centrifugation (15 000 rpm, 20 min).[28] The washed cell wall was suspended in 1 mL 25 mM NaH_2PO_4 pH 6.0, 10 mM $MgCl_2$ and digested with DNase and RNase for 2 h at room temperature with mixing, followed by the addition of proteinase K and further incubation for 18 h at room temperature with mixing. Following proteinase K digestion, the sample was centrifuged (15 000 rpm, 20 min) and the pellet resuspended in 1 mL of 25 mM NaH_2PO_4 pH 6.0 with 4% SDS and heated at 95 °C for 30 min in a hot block. The purified PG was isolated by centrifugation (15 000 rpm, 20 min) and washed extensively in phosphate buffer to remove residual SDS. The resulting pellets were stored at −20 °C.

Preparation of peptidoglycan fragments and analysis by HPLC

Purified PG pellets were resuspended in 1 mL of 25 mM NaH_2PO_4 pH 6.0 by sonication and standardized to OD_{600nm} prior to digestion with 100 units of mutanolysin overnight at 37 °C with agitation. Insoluble fragments were removed by centrifugation (15 000× rpm, 20 min) and the supernatant transferred to a new microcentrifuge tube. The soluble muropeptides were reduced with sodium borohydride in 0.1 M sodium borate buffer pH 9 for 30 min. The reaction was quenched by the addition of 1 M H_3PO_4 to a final pH of 5 (litmus paper). The reduced muropeptides were filtered through a 5 kDa MWCO spin column prior to analysis. The reduced muropeptides were separated by RP-HPLC on a Shimadzu Prominence HPLC equipped with a Phenomenex Kinetix C-18 column (5 μm, 100 A, 250 × 4.6 mm) equilibrated in 10 mM $NH_4H_2PO_4$ pH 5.6 (buffer A). Muropeptides were eluted with a linear gradient of methanol (0–20%) in buffer a over 200 min with detection at 205 nm.[29]

LCMS analysis of muropeptides

Reduced muropeptides were separated by an Advion Avant UPLC system equipped with an Interchim Ultisphere CS Evolution C18 column (2.6 μm, 100 × 2.1 mm) and paired with an Advion compact mass spectrometer with electrospray ion

source. The column was equilibrated in 98% solvent A (H_2O + 0.1% formic acid) and 2% solvent B (MeOH + 0.1% formic acid). Muropeptides were eluted with the following gradient over 30 min: 98% A hold for 3 min, 93.2% A 6 min; 91% A 7.5 min; 86% A 9 min; 80% A 11 min; 10% A 25 min, hold at 10% A for 5 min. MS detection was set for switching positive and negative ion mode.

Incorporation of fluorescent D-amino acid HADA into cell wall

B. subtilis wildtype and knockout strains were passaged three times using 1/100 inoculum at 37 °C with shaking. Overnight culture was used to inoculate a 50 mL flask of LB 1/100 and grown with shaking at 37 °C to an $O.D._{600nm}$ = 0.2. The cells were then split into 1 mL samples containing either 1 mM HADA (7-hydroxycoumarin-3-carboxylic acid-D-alanine)[30] or 1 mM HADA with 0.75× MIC (3 μM) Mas. Cells were grown for 1 h at 37 °C with shaking, followed by addition of Syto-13 (final concentration 1 μM) and harvesting the cell pellets by centrifugation (9000 rpm, 10 min). The cell pellets were washed 3 × in ice cold 25 mM NaH_2PO_4 pH 7.5, 100 mM NaCl (PBS). Washed cell pellets were suspended in PBS and 40 μL was mixed with 10 μL Diamond anti-fade prior to spotting onto microscope slides for visualization by confocal fluorescence microscopy (see below).

Fluorescence microscopy

Phase and fluorescence images were acquired using a Zeiss LSM-laser scanning microscope equipped with a objective 40× objective. Zeiss software was used for image acquisition. Images were scaled without interpolation, cropped and rotated. Linear adjustment was performed to optimize contrast and brightness of the images. Figure construction was performed in CorelDraw.

Electron microscopy

Washed and resuspended bacterial cells were pipetted in 10 μL drops onto parafilm. Formvar, carbon coated, 400 mesh, copper grids were floated on top of the droplets for 1 min, floated on 50 μL drop of double distilled water for 1 min, and then floated on 50 μL drops of 1% uranyl acetate in double distilled water for 1 min. Grids were picked up with tweezers and the excess uranyl acetate wicked of onto Whatman filter paper. Grids were place in a grid box, which was left open overnight to allow samples to dry. Samples were viewed and imaged with a Jeol JEM-200 CX transmission electron microscope and an AMT camera. For thin-section microscopy, bacterial samples were pelleted by centrifugation. Pellets were resuspended in 4% paraformaldehyde and 2% glutaraldehyde in phosphate buffered saline (PBS) and incubated at 4 °C overnight. Samples were washed 3 × 10 minutes in 0.1% sodium cacodylate. Samples were stained in 1% osmium tetroxide in 0.1% sodium cacodylate for 1 hour. Samples were washed 3 × 10 min in distilled water. Samples were stained in 1% uranyl acetate in water at 4 °C overnight. Samples were dehydrated in a graded series of ethanol of 50, 75, 85, 95%, in water for 30 minutes each. Samples were washed with 3 changes of 100% ethanol for 30 minutes each. Samples were incubated in 50, 75, 100, 100% spurr embedding resin overnight for each step. Samples were pipetted into an embedding capsule with fresh 100% resin and the capsules placed in an oven at 80 °C for 48 hours. Samples were sectioned at 70 nm and section collected on formvar carbon coated copper EM grids. Samples were visualized and imaged using a Jeol CX200 transmission electron microscope and an AMT camera.

Atomic force microscopy

Second passage bacterial cells were grown to $OD_{600\ nm}$ = 0.2 in LB broth and incubated in the presence/absence of masarimycin (3 μM, 0.75× MIC) for 2 h with shaking at 37 °C. Cells were fixed with ethanol (final concentration of 20% (v/v)) and incubated on ice for 20 min. Cells were harvested (5000 rpm, 10 min, 4 °C) and washed twice with PBS. Cells were resuspended in dH_2O and 10 μL spotted on a glass coverslip. Images were recorded on a Redux AFM (ICSPI Corp, Kitchener, ON Canada).

4-Nitrophenyl-*N*-acetyl-β-D-glucosaminide assay

B. subtilis second passage cells were grown in LB broth at 37 °C with shaking to an OD_{600nm} = 0.2 and the cells harvested by centrifugation (8000 rpm, 10 min). The cells were washed twice in PBS prior to re-suspending in PBS to an OD_{600} of 1.0. All reactions contained 4 mM pNP-GlcNAc and 198 μL of *B. subtilis* cells (OD_{600nm} = 1.0) in PBS buffer pH 7.4. Reactions were incubated for 16 h at 30 °C prior to removal of cells by centrifugation (8000 rpm, 10 min). Reaction supernatants were adjusted to pH 9 with the addition of 30 μL NaOH (0.5 M). Supernatants were then analyzed on a Spectromax 190 microtitre plate reader (Molecular Devices) at 405 nm. All samples were run in biological duplicate and technical triplicate.

Macromolecular synthesis assay

Inhibition of macromolecular synthesis by masarimycin was monitored by flow cytometry.[31] Overnight bacterial cultures were sub-cultured 1/20 into fresh media and grown to exponential phase growth. Bacterial cultures were incubated with antibiotics, vehicle control, or masarimycin ranging in concentration from 1/4 to 2× MIC for 1 h. For analysis of total protein content, cells were incubated with Sypro-red for 4 min. Total nucleic acid content was measured by incubation with Syto-13 (9 μM) 15 min. Changes to transmembrane potential were measured with DiSC3.[31] Stained cells were analyzed by flow cytometry performed on a Cytek Aura.

Results

Morphological changes induced by masarimycin – electron and atomic force microscopy

We have previously shown that sub-MIC Mas-treated *B. subtilis* exhibit a sausage-link phenotype.[19] To better understand the physiological changes that give rise to this morphology, cells were investigated by negative stain and thin-section electron

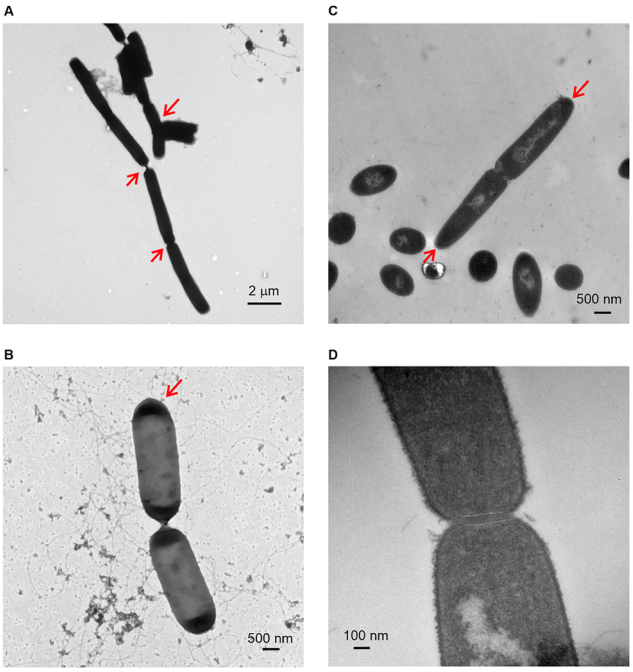

Fig. 2 Electron microscopy of *B. subtilis* treated with 0.75× MIC (3 μM) Mas. (A) and (B) Negative stain EM showing elongated cells and incomplete septation; (C) and (D) thin section EM showing accumulation of cell wall material at the poles of Mas treated cells.

microscopy (Fig. 2). Masarimycin induces a morphology in which *B. subtilis* cells are elongated, along with an inability to complete the separation of daughter cells. The average cell length of 15 μm, is 3 times greater than typical wildtype *B. subtilis* cells. Cells presented a pronounced cleavage furrow (Fig. 2B) indicating an inability to complete constriction of the septum and electron dense regions at the poles suggest a thinkening of the cell wall (Fig. 2B). This is further supported in thin-section images (Fig. 2C and D) demonstrating thickened cell wall at the poles. Additionally, electron microscopy identified cells with abberant division planes, with daughter cells formed from the sidewall instead of the poles (Fig. 2A and Fig. S1). These observations suggest that Mas either directly or indirectly interferes with localization of the FtsZ ring. Further analysis of changes to the cell surface of *B. subtilis* by atomic force microscopy indicate a roughening of the cell surface, consistent with abberant autolytic activity or an altered distribution of wall teichoic acids (Fig. 3).

Effect of masarimycin on PG metabolic labeling

Given the disruption in cell shape and impaired separation of daughter cells, we further evaluated the changes to PG metabolism *via* metabolic labeling with the fluorescent D-amino acid analog HADA.[30,32] HADA is incorporated exclusively into muropentapeptides at the fifth position *via* an extracellular mechanism using predominantly D,D-transpeptidases.[30,32] Additionally, HADA does not appear to be incorporated when the D-Ala in the fourth position is involved in a cross-link.[32] Early exponential phase *B. subtilis* (OD_{600nm} = 0.2) were incubated with 1 mM HADA for 1 h in the presence of 3 μM Mas (0.75× MIC) or vehicle control (DMSO), and imaged by confocal microscopy. Control wild type cells demonstrated incorporation of HADA into the cell wall with distribution along the sidewalls (Fig. 4A) with actively dividing cells showing an increased accumulation of HADA at division sites. In the presence of 0.75× MIC Mas (Fig. 4B), HADA fluorescence is weaker, indicating there is an overall loss of HADA incorporation, along with a lack of incorporation at septa. Previous work has shown that septa in *B. subtilis* are enriched in unprocessed pentapeptides, indicating a reduction in cross-linked PG at the division site.[33] The reduced HADA signal in the presence of Mas could result from either decreased D,D-transpeptidase activity or an increase in the presence of cross-linked glycan strands.

While HADA is incorporated into stem-peptides *via* D,D-transpeptidases, it can also be removed *via* the action of carboxypeptidases like DacA (Pbp5).[30] To further investigate whether the reduction in HADA incorporation in the presence

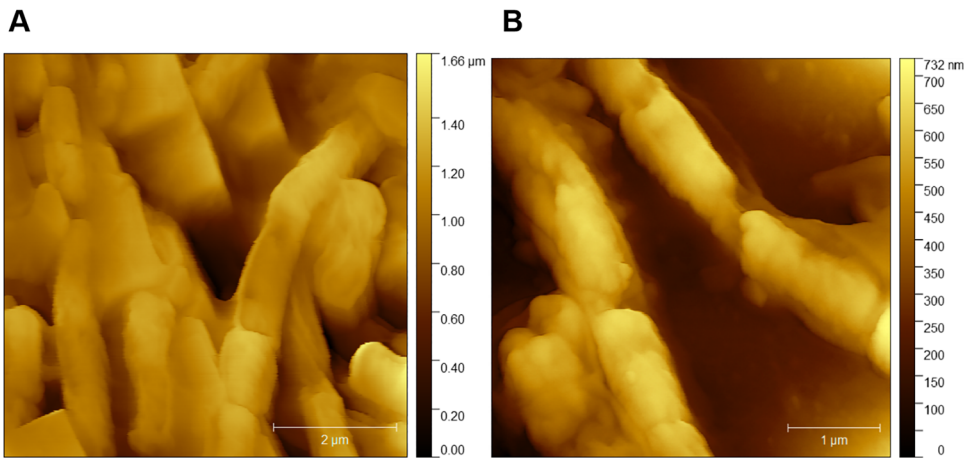

Fig. 3 Atomic force microscopy of *B. subtilis* control (A) and 0.75× MIC masarimycin treated (B) cells. Treatment with masarimycin results in a rough surface that correlates with the observed thickening of the cell wall in thin-section electron microscopy images.

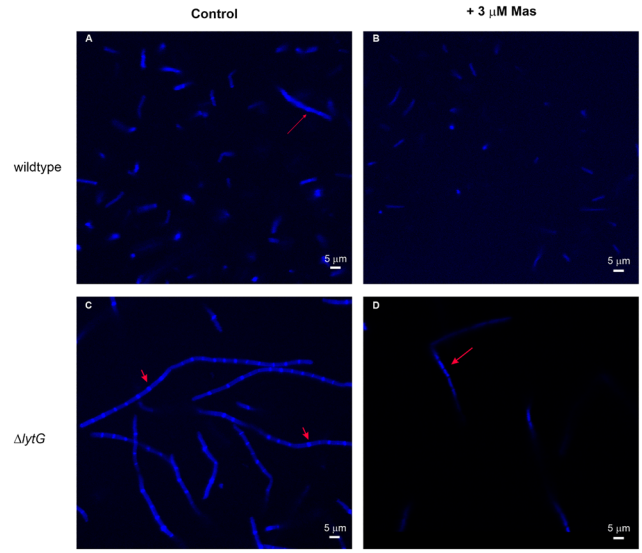

Fig. 4 Confocal fluorescence microscopy (40× objective) of *B. subtilis* cell wall stem-peptides metabolically labeled with HADA. Early exponentially growing *B. subtilis* cells ($OD_{600\ nm}$ = 0.2) labeled with 1 mM HADA and Syto-13 in the absence (A) and (C) or presence (B) and (D) of 0.75× MIC Mas.

of Mas is due to cleavage of the HADA group by carboxypeptidases such as DacA, we investigated HADA incorporation in Δ*dacA* and *ΔlytG* backgrounds. In the absence of DacA (Fig. S2B), diffuse incorporation of HADA was observed throughout the control sample, consistent with prior observations of this mutant.[30,32] Additionally, there is a complete absence of HADA incorporation at septa. Mas-treated *ΔdacA* cells demonstrated increased HADA fluorescence throughout the cell including at septa. Fluorescence was stronger in the Mas treated *ΔdacA* cells than in either the *ΔdacA* or wildtype control cells. This nullifies the hypothesis that reduced HADA incorporation in Mas treated wildtype cells is due to an increase in DacA carboxypeptidase activity. Furthermore, these results suggest that there is an increase in D,D-transpeptidase activity in the *ΔdacA* strain when LytG is inhibited by Mas. In comparison, the *ΔlytG* mutant demonstrates diffuse HADA incorporation along the side walls with HADA incorporation concentrated at septa (Fig. 4C and D). Labeling with HADA appears to result in a chaining phenotype in *ΔlytG* that does not appear in unlabeled cells (Fig. S3). This is also observed in the wild type Mas treated cells where the Mas-induced phenotype is less pronounced. Upon treatment of *ΔlytG* with Mas, the concentrated HADA labeling at the septa disapears and overall fluorescence decreases (Fig. 4D). This is an intriguing result, as Mas should not have any impact on cells that lack its target protein LytG. This result in the *ΔlytG* strain suggests incomplete suppression of LytG activity. The results presented here also indicate a coordination of activity between LytG, DacA and D,D-transpeptidases.

Muropeptide analysis

With the observed changes in HADA incorporation in Mas-treated cells in the Δ*dacA* and Δ*lytG* strains, the muropeptide

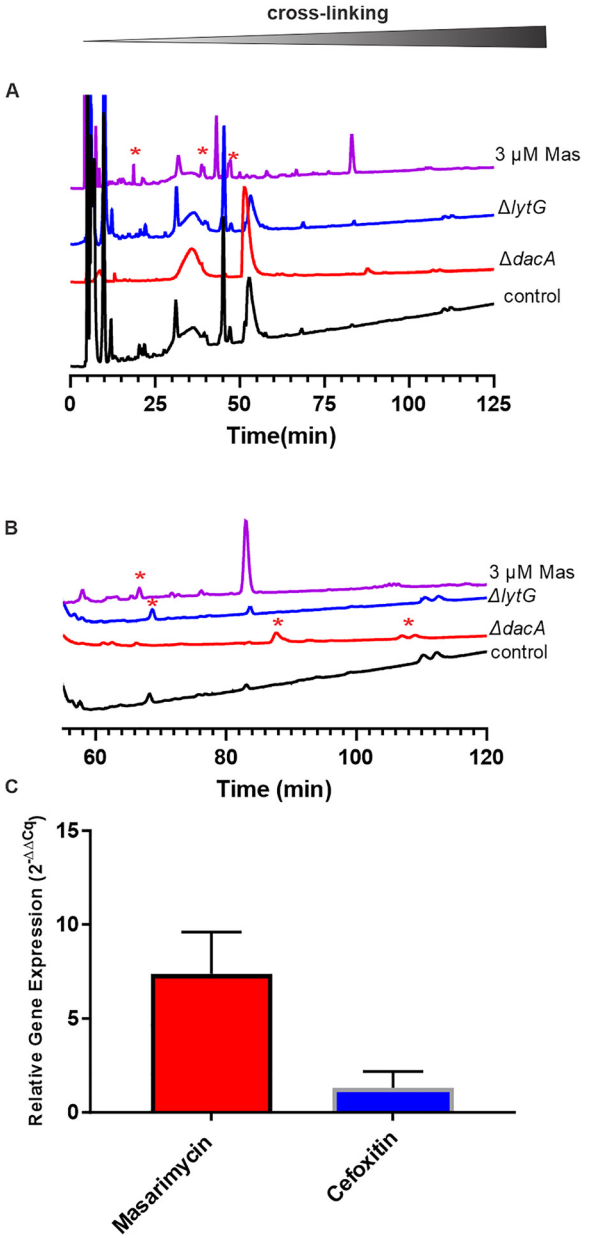

Fig. 5 (A) RP-HPLC muropeptide profile of *B. subtilis* in the absence or presence of Mas and comparison to the *ΔlytG* and Δ*dacA* strains. (B) RP-HPLC muropeptide profiles in the 60–120 min region. (C) Relative quantitation of *relA* (ppGpp) synthase as a measure of induction of stringent response upon treatment with Mas or the cell wall antibiotic cefoxitin. Experiments were run in biological and technical duplicate. Average $2^{-\Delta\Delta Cq}$ with standard deviation are presented. Asterisk denotes unique muropeptides.

profiles were analyzed (Fig. 5A and B). Given the number of D,D-transpeptidases encoded by *B. subtilis*,[34,35] this approach allowed for the assessment of global transpeptidase activity in Mas-treated cells. Additionally, this further assessed whether changes in HADA incorporation are in part due to changes in cross-linking. *B. subtilis* was grown to early exponential phase (50 mL LB, OD_{600nm} = 0.2) and treated with 0.75× MIC Mas or vehicle control. After 2 h incubation, cells were harvested and

PG was isolated using established procedures.[27] Soluble muropeptides were obtained by digestion with mutanolysin followed by reduction of reducing ends with sodium borohydride. Separation of muropeptides by RP-HPLC was achieved using a linear gradient of 10 mM $(NH_4)_2HPO_4$ pH 5.6 containing 20% methanol.[29] Muropeptide profiles of Mas-treated cells showed an increase in cross-linking (Fig. 5B) (longer retention times) compared to control cells.[29] It should be noted that mutanolysin cleaves the MurNAc-β(1 → 4)-GlcNAc linkage only when the MurNAc residue bears a pentapeptide, further supporting the increased cross-linking hypothesis.[36] This increased cross-linking would impair transpeptidase reactions where HADA is used as a substrate. Interestingly, the muropeptide profile of Mas treated cells are distinct from *ΔlytG* and *ΔdacA* muropeptide profiles. LCMS analysis of muropeptides (Table 1) reinforces this finding. Mas treated *B. subtlis* shows a significant reduction in identified monomers and an increase in unique dimers and tetramers compared to wild type. A reduction in monomers was also observed in the *ΔlytG* and *ΔdacA* strains.This increased cross-linking would impair transpeptidase reactions where HADA is used as a substrate. Interestingly, the muropeptide profile of Mas treated cells are distinct from *ΔlytG* and *ΔdacA* muropeptide profiles. The increased cross-linking in the presence of Mas also demonstrates that it does not inhibit transpeptidase or carboxypeptidase activity. These results support the hypothesis that the reduction of HADA incorporation upon Mas treatment is in part due to increased cross-linking of the cell wall.

Cell wall stress response

The apparent disregulation of PG metabolism, manifesting as a thickened and irregular cell wall with increased cross-linking in response to Mas, raises the question of whether the cell wall stress response is induced upon exposure of *B. subtilis* to Mas. The bacterial alarmone (p)ppGpp acts as an important second-messenger linking both intra- and extracellular environmental cues with global changes in transcription.[37] In *B. subtilis* (p)ppGpp levels are predominantly controled by the bifunctional synthase/hydrolase RelA and can serve as a reporter for cell wall stress.[38,39] Levels of (p)ppGpp have been shown to influence Sigma D (SigD) controlled genes and high levels of (p)ppGpp are associated with the stringent response.[37] Several SigD controlled autolysins (LytD, LytC, LytF)[40] have been shown to influence sensitivity to Mas.[19] Primers for *relA* produced a single product of 97bp and demonstrated a linear response to

Table 1 Unique muropeptides identified by LCMS for *B. subtilis* 11774 in the absence and presence of Mas, and the mutant strains *ΔlytG* and *ΔdacA*

Ion	Observed *m/z*	Calculated *m/z*	Δ*m/z*	Muropeptide composition[a]
WT				
		Monomers		
$[M + 3H]^{+3}$	339.3	338.7	0.63	$(GlcNAc)_1(MurNAc)_1Ala_3Glu_1A_2pm_1$
$[M-2H]^{-2}$	556.0	556.0	0	$(GlcNAc)_1(MurNAc)_1Ala_2Glu_1A_2pm_1$
$[M + Cl]^{-1}$	1034.1	1034.3	0.02	$(GlcNAc)_1(MurNAc)_1Ala_2Glu_1A_2pm_1Gly_1$
$[M + K-2H]^{-1}$	908.0	909	1.0	$(GlcNAc)_1(MurNAc)_1Ala_1Glu_1A_2pm_1$
		Dimers		
$[M + 3H]^{+3}$	646.4	646.6	0.23	$(GlcNAc)_2(MurNAc)_2Ala_5Glu_2A_2pm_2$
$[M + Na-2H]^{-1}$	1815.9	1815.8	0.01	$(GlcNAc)_2(MurNAc)_2Ala_3Glu_2A_2pm_2$
$[M-H_2O-H]^{-1}$	1846.6	1846.9	0.01	$(GlcNAc)_2(MurNAc)_2Ala_4Glu_2A_2pm_2$
		Trimers		
$[M-4H]^{-4}$	710.6	710.4	0.02	$(GlcNAc)_3(MurNAc)_3Ala_6Glu_3A_2pm_3Gly_1$
		Tetramers		
$[M-2H]^{-2}$	1890.4	1890.3	0.1	$(GlcNAc)_4(MurNAc)_4Ala_9Glu_4A_2pm_4$
WT + Mas				
		Dimers		
$[M + 2Na-H]^{+1}$	1843.3	1839.7	3.5	$(GlcNAc)_1(MurNAc)_2Ala_3Glu_2A_2pm_2$
$[M-6H]^{-6}$	318.7	319.5	0.8	$(GlcNAc)_2(MurNAc)_2Ala_6Glu_3A_2pm_3Gly_1$
$[M + 3H]^{+3}$	623.0	622.9	0.01	$(GlcNAc)_2(MurNAc)_2Ala_4Glu_2A_2pm_2$
		Tetramers		
$[M + 5H]^{+5}$	757.8	757.5	0.3	$(GlcNAc)_4(MurNAc)_4Ala_9Glu_4A_2pm_4$
ΔlytG				
		Monomers		
$[M-2H]^{-2}$	556.1	556.0	0.1	$(GlcNAc)_1(MurNAc)_1Ala_2Glu_1A_2pm_1$
		Trimers		
$[M + 4H]^{+4}$	712.3	712.4	0.1	$(GlcNAc)_3(MurNAc)_3Ala_6Glu_3A_2pm_3Gly_1$
$[M + 4H]^{+}4$	680.6	680.4	0.2	$(GlcNAc)_3(MurNAc)_3Ala_5Glu_3A_2pm_3$
ΔdacA				
		Monomers		
$[M + 4H]^{+4}$	218.9	218.7	0.2	$(GlcNAc)_1(MurNAc)_1Ala_1Glu_1A_2pm_1$
		Dimers		
$[M + Na]^{+1}$	1960.0	1959.9	0.1	$(GlcNAc)_2(MurNAc)_2Ala_5Glu_2A_2pm_2$
$[M + 2H]^{+2}$	900.3	898.4	−1.9	$(GlcNAc)_1(MurNAc)_2Ala_3Glu_2A_2pm_2$
$[M-3H]^{-3}$	640.1	639.9	−0.13	$(GlcNAc)_2(MurNAc)_2Ala_4Glu_2A_2pm_2Gly_1$

[a] A_2pm: diaminopimelic acid.

template concentration (Fig. S4). Incubation in the presence of masarimycin for 20 min showed a 7-fold increase in *relA* transcript levels (Fig. 5C). The β-lactam cefoxitin was used as the positive control for cell wall stress response.

Effect of Mas on cell wall knockouts

In light of the changes to the cell wall and induction of cell wall stress response, we wanted to investigate potential Mas-altered fitness using a chemical genetics interaction approach. Previously we screened several *B. subtilis* SigD controlled autolysins (LytC/D/F) for changes in fitness to Mas, all of which showed increased sensitivity.[19] These results suggested that the GlcNAcase (LytD), amidase (LytC), and endopeptidase (LytF) are conditionally required for adaptation to Mas exposure. Given the clear disruption in cell division and peptidoglycan metabolism in the presence of Mas, an array of *B. subtilis* strains lacking autolysins including GlcNAcase, carboxypeptidase, transpeptidase, and cell wall division proteins (MinC/D) were screened for altered fitness to Mas (Fig. 6A).

Given the previous biochemical evidence indicating Mas inhibits the exo-GlcNAcase LytG,[19] along with the reduction in *p*-nitrophenol release in the presence of Mas in a whole cell assay (*vide infra*, Fig. 6), the observation that the Δ*lytG* mutant strain demonstrates reduced sensitivity (increased fitness) to Mas with no MIC observed up-to a concentration of 40 μM (10× wild type MIC) is in line with those results. The Δ*lytG* strain does not produce the characteristic sausage-linked phenotype in the presence of up to 24 μM Mas (6× MIC) (Fig. S3A and B).

Interestingly, several additional autolysins, transpeptidases, and cell division mutants also exhibited increased fitness to Mas. The class A (bifunctional) PbpA (PBP2a) and the class B PbpH are implicated in elongation and rod shape determination, which given the Mas-induced phenotype is suggestive of their involvement.[41] Analysis of morphology changes upon Mas treatment of Δ*pbpA* indicated an increase in irregular cell shapes, with the presence of a bulge in the side wall (Fig. S3C and D). This bulge was more prominently observed in Mas treatment of *ΔpbpD* and *ΔminC* strains (Fig. S3G–J). The *ΔminC* strain also shows a reduction in cell clumping upon treatment with Mas. The observed bulge is reminiscent of the phenotype induced in *E. coli*, upon co-treatment with bulgecin (an inhibitor of the soluble lytic transglycosylase 70) and a β-lactam.[42–44] The phenotypes presented in Mas-treated *B. subtilis* wildtype and mutant strains (Fig. 2 and Fig. S3) and the apparent inability to complete separation of daughter cells led us to screen mutants strains lacking cell division associated proteins MinC, MinD,and FtsH. All strains demonstrated increased fitness to Mas (Fig. 6A).

While this broad based improved fitness to Mas with elongation and division associated proteins argues that Mas is targeting cell wall acting proteins, it is also possible that these effects arise from a non-specific Mas-induced disruption of membrane polarization or impact global protein, or nucleic acid levels in the cell. Given this potential promiscuity of Mas, we screened *B. subtilis* for disruption in membrane polarization, total protein and nucleic acid synthesis by flow cytometry

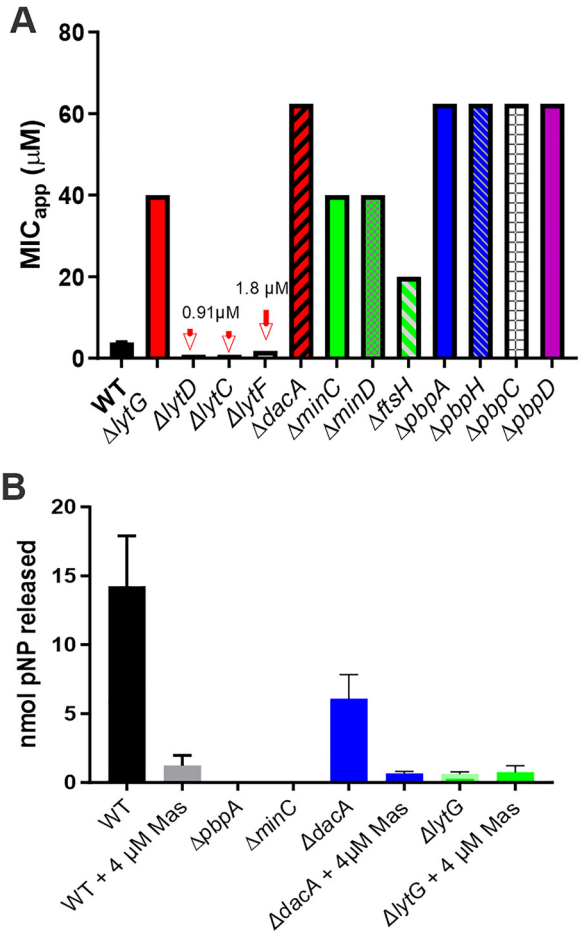

Fig. 6 (A) Chemical genetic screen of autolysin (*lytG*, *dacA*) cell division (*minC*, *minD*, *ftsH*), and transpeptidases (*pbpA*/*H*/*C*/*D*) mutant strains for changes in Mas sensitivity. (B) Whole cell assay measuring exo-GlcNAcase activity in several mutant strains from the genetic screen. Results shown are the average of 2 biological and technical replicates.

(Fig. S4). In all cases, no disruption to membrane polarization or protein synthesis was observed up to 2× MIC. This supports an argument that Mas inhibition of LytG results in disregulation of elongation and division complexes in *B. subtilis*.

A direct biochemical explanation for the increased fitness to Mas in these genetic backgrounds is a reduction in exo-GlcNAcase (LytG) activity in these strains. To explore this further, wildtype *B. subtilis* and *ΔpbpA*, *ΔminC*, *ΔdacA*, and *ΔlytG* strains were subject to a whole cell exo-GlcNAcase activity assay.[18] *B. subtilis* cells were grown to early exponential phase, washed in PBS and incubated with 4 mM pNP-GlcNAc for 16 h, followed by measurement of released pNP (Fig. 6B). As expected, exo-GlcNAcase activity of wild-type was reduced in the presence of Mas. Additionally, the *ΔlytG* strain exhibited residual exo-GlcNAcase activity which supports the argument that complete abbrogation of *exo*-GlcNAcase activity is not achieved in the *ΔlytG* knockout. In the *ΔdacA* strain a significant reduction in exo-GlcNAcase activity was observed compared to wildtype cells. Upon treatment with 4 μM Mas, *exo*-GlcNAcase activity was further reduced due to inhibition. This suggests that

the observed improved fitness to Mas in the *ΔdacA* strain is in part due to a reduction in exo-GlcNAcase activity in these strains.

Checkerboard assays with Mas

Given the complex interactions at play upon Mas inhibition of *B. subtilis* growth through the inhibition of LytG, and the complicated results from the genetic screen and HADA labeling experiments, Mas was screened in checkerboard assays to identify potential synergistic or antagonistic relationships with antibiotics with well-defined modes-of-action (Table 2).[24,25,45] Synergistic interactions can reveal functional connections among cellular components,[24] while antagonistic interactions can reveal underlying network connectivity.[46] Synergy was observed with ampicillin (FIC_{Index} 0.134), a PBP2a/b (encoded by *pbpA*/*H*) and PBP4 selective β-lactam;[47] and vancomycin (FIC_{Index} 0.235) which binds to the terminal D-Ala-D-Ala in lipid-II and interferes with the PG maturation process.[48] Vancomycin binding obstructs PBP cross-linking activity, resulting in a compromised cell envelope integrity. In light of the information that the cellular response to Mas treatment is an increase in cross-linking, this functional connection with PG maturation further strengthens a cell wall mode-of-action. Synergy was also observed with curcumin (FIC_{Index} 0.00375), an inhibitor of FtsZ protofilament assembly,[49] and reversatrol (FIC_{Index} 0.127) an inhibitor of FtsZ expression and Z-ring formation.[50] These results correlate with the Mas induced sausage-link phenotype and disrupted division (Fig. 2).[19] These results demonstrate a functional connection between the Mas target and the effective assembly of the Z-ring.

Antagonism was observed with bacitracin (FIC_{Index} 5.88) an inhibitor of undecaprenyl-pyrophosphate recycling, cefuroxime (FIC_{Index} 4.91) a PBP1 selective β-lactam,[47] and kanamycin (FIC_{Index} 4.89) a protein synthesis inhibitor (30 s subunit). PBP1 serves as the major transglycosylase/transpeptidase in the cell and is associated with the cell elongation and division complexes in *B. subtilis*.[51] Bacitracin's interference with undecaprenyl phosphate recycling impacts the biosynthesis of both PG and wall teichoic acids. Wall teichoic acids have been shown to play a role in guiding cell wall interactions through the CHAP domains of autolysins.[52,53] Additionally, wall teichoic acids are known to physically restrict the exposure of peptidoglycan to autolysins and ensure limited PG digestion at the septa during cell division and separation.[54,55] Finally, disruption in teichoic acids have been shown to influence autolytic activity in a variety of bacteria including *B. subtilis*.[56,57] Bacitracin would impede synthesis of new lipid II by preventing recycling of Und-PP while cefuroxime would inhibit PG incorporation into the existing cell wall. The antagonism with kanamycin was an intriguing result. While Mas does not interfere with total protein levels in the cell (Fig. S4), kanamycin has previously been shown to confer short-term protection to a variety of functionally unrelated antibiotics, including β-lactams.[58] Additionally, the induction of cell wall stress reponse (RelA) and (p)ppGpp production has been shown to result in the direct inhibition of translation through inactivation of GTPase initiation factor-2.[59]

To further interrogate disruption of PG metabolism, we examined the role of sugar intermediates associated with PG biosynthesis and assembly and whether they synergized or antagonized Mas sensitivity. Interestingly, addition of glucosamine to the culture media (3 μM) lowered the apparent MIC of Mas to 0.244 μM a 16 fold increase in sensitivity. This result suggests potential toxicity of GlcN, nitrogen toxicity, or feedback inhibition of cell wall precursor biosynthesis during Mas

Table 2 Synergy and antagonism screen with masarimycin

Antibiotic	MIC_{app} antibiotic (μM)	FIC antibiotic	MIC_{app} Mas[a] (μM)	FIC mas	FIC index[b]
Cell-wall targeting					
Ampicillin	3.12	0.0975	0.460	0.121	0.134
Cefoxitin	4.70	1.04	5.85	1.54	2.59
Cefuroxime	0.49	0.035	18.5	4.87	4.91
Bacitracin	577.5	3.30	10.0	2.63	5.88
Vancomycin	0.293	0.073	0.62	0.164	0.235
Fosfomycin	18.75	2.60	1.40	0.367	2.97
Cell division					
Curcumin	0.0001	0.0000023	0.015	0.00375	0.00375
Reversatrol	1	0.005	0.488	0.122	0.127
Protein synthesis					
Kanamycin	0.03	2.3	2.31	0.60	4.89
Tetracycline	0.0035	1.25	0.28	0.073	1.8215
Nucleic acid synthesis					
Rifampicin	0.08	0.96	3.9	1.03	1.99
Sugar intermediates					
GlcN	n.d.[c]	—	0.244[d]	—	—
GlcNAc	n.d.	—	4.0 μM	—	—
MurNAc	n.d.	—	4.0 μM	—	—

[a] MIC masarimycin 4.0 μM. [b] FIC index: <0.5 – synergistic; >0.5–1 – additive; >1–4 – indifference; >4 – antagonistic. [c] No MIC observed. [d] MIC_{app} for masarimycin in the presence of 3 μM GlcN.

treatment. To pursue the feedback inhibition hypothesis, we conducted checkerboard assays in the presence of GlcNAc and MurNAc, two downstream sugar intermediates in PG biosynthesis. In both cases, no alteration in Mas activity was observed. This suggests that feedback inhibition is the the cause of the observed GlcN sensitivity.

Discussion

Unravelling the physiological changes that give rise to the Mas phenotype using a combination of chemical biology and genetic approaches has highlighted the complexity of peptidoglycan and cell wall metabolism. Based on negative staining EM, genetic screening, and synergy/antagonism assays, our data shows a connection between Mas treatment and the disruption of proper FtsZ ring formation and localization. We have shown that Mas inhibition of LytG results in a thickening of the cell wall and roughening of the cell surface (Fig. 2 and 3) and disruption of cell division and division plane (Fig. 2 and Fig. S1), indicating that Mas impacts the divisome. Support for this can be found in the observed synergy of Mas with the FtsZ binding compounds curcumin and reversatrol. Thickening poles (Fig. 2B and C) could arise from perturbations to the activity of SepF, which binds to FtsZ and plays a role in the correct assembly of the cross-wall septum (Fig. 7).[60,61] Disrupted septum assembly and function is also supported by the EM (Fig. 2) and HADA incorporation experiments (Fig. 4). The increased fitness to Mas in the *ΔminC* mutant also implicates FtsZ, as the localization of the FtsZ ring at the mid-cell is in part controlled by MinC, which prevents FtsZ ring formation at the poles and regulates the timing of cell division.[62]

Metabolic labelling with HADA in wild type and *ΔlytG* was impaired in the presence of Mas, while in the Δ*dacA* strain increases in HADA incorporation and distribution were observed with Mas (Fig. 4B and C, Fig. S2). The Mas-induced decrease in HADA incorporation in the *ΔlytG* strain could arise from incomplete knockout of the gene, supported by the residual GlcNAcase activity observed in *ΔlytG*. Further complicating the genetic screen results is the finding that several of the deletion strains also exhibit a decrease in *exo*-GlcNAcase activity, suggesting that part of the cause in the observed increased fitness is a decrease in the confirmed target LytG. These results indicate that the phenotypes observed in single genetic knockout strains are not necessarily the result of a single gene but arise from more complex pleiotropic effects in

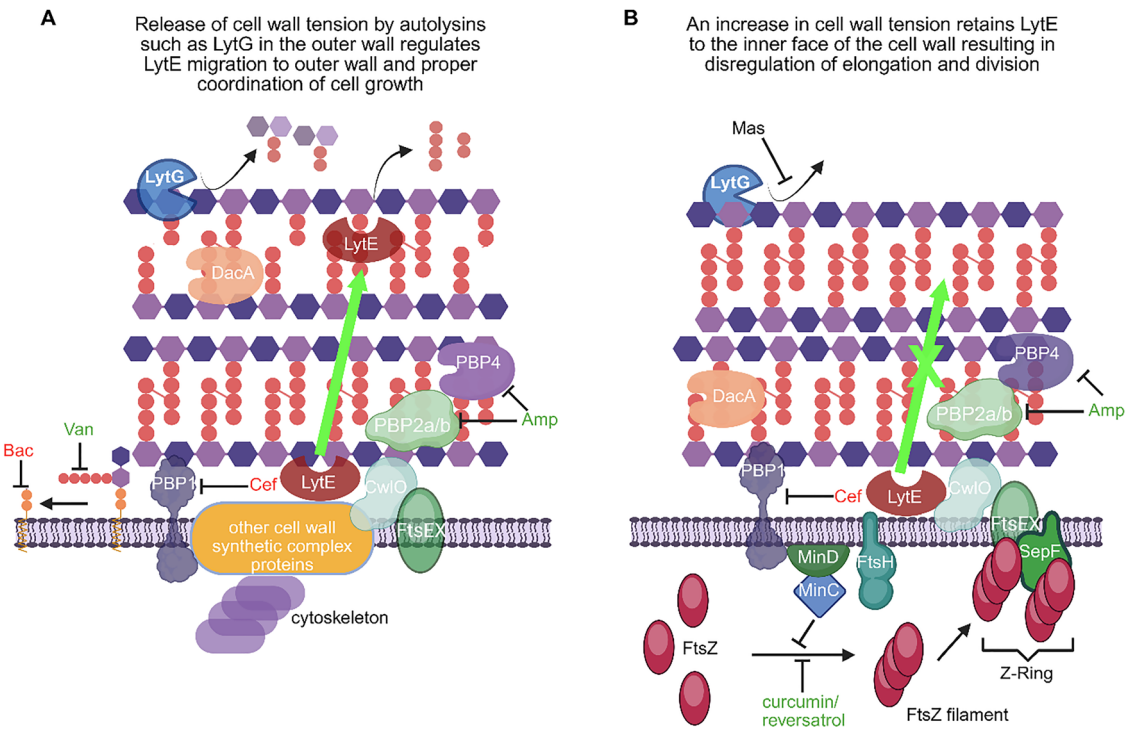

Fig. 7 Proposed mechanism of Mas-induced phenotypes through the inhibiton of the the *exo*-acting GlcNAcase LytG. Antiobiotics demonstrating synergy with masarimcyn are shown in green while antagonistic relationships are shown in red; Bac: bacitracin, Van: vancomycin, Cef: cefoxitin, Amp: ampicillin, Mas: masarimycin (A) Under normal growth conditions there is tight coordination between biosynthesis and degradation of PG. PG hydrolases such as LytG release tension in the outer layers of the cell wall releasing soluble muropeptides this allows for the migration of the essential endopeptidase LytE to migrate from the inner to the outer wall as the cell grows. This leaves the other essential endopeptidase CwlO as an integral part of the elongation and divison complexes. (B) In the presence of masarimycin, LytG is inhibited preventing the release of tension in the outermost layers of the cell wall. This prevents the outward migration of LytE as nacent PG is no longer pulled into the stress-bearing layers. This results in LytE being retained in the cell wall synthetic complex, resulting in disregulated growth and division manifesting in part by changes in cross-linking through the activity of DacA and D,D-transpeptidases (D,D-TP). Created in **https://BioRender.com**.

response to the gene deletion. This highlights the cautionary note that the lack of a simple 1-to-1 relationship between target and inhibitor in observed outcomes can complicate the interpretation of results from screening of cell wall active compounds against single mutants.

Bacterial cell wall assembly during cell division and cell growth is regulated by multiple-protein complexes – the division complex (divisome) and the elongation complex (elongasome). These complexes control the activity of various autolytic enzymes required to cleave glycosidic or peptidic bonds during the growth and remodeling of peptidoglycan. Our observations provide additional evidence for the link between autolysin activity and divisome and elongasome activity. This link, which is well established for the essential D,L-endopeptidases LytE and CwlO, highlights the need for a tight balance between PG synthesis and hydrolysis.[63] CwlO is activated by the membrane protein complex FtsEX, requires the actin-like protein MbI for function, and is restricted to the inner part of the cell wall. CwlO activity is tightly coordinated with PG synthases.[64]

Unlike CwlO, LytE regulation is less well understood. At the membrane, LytE is regulated in part by MreB and MreBH of the cell division apparatus. LytE possesses a cell wall binding domain that facilitates migration to the outer stress bearing layers as the cell wall matures. It has been postulated that in *B. subtilis* the autolysin LytE is a stress response factor that is recruited to the elongation complex and interacts with MreB/MreBH when cell expansion is compromised.[64] In the absence of LytE, CwlO acts as the major elongation endopeptidase, with PG synthesis well-coordinated with turnover and normal growth achieved. When LytE is the major endopeptidase in the biosynthesis complex regular growth and turnover is impaired.

The data presented here shows that upon treatment with Mas, *B. subtilis* experiences compromised cell expansion, resulting in the activation of the cell wall stress response (*via* alarmone (p)ppGpp). Since LytG is the major active GlcNAcase during vegetative growth,[21] we speculate that inhibition by Mas results in impaired release of tension in the outermost layers of the cell wall, impeding the outward migration of LytE and keeping it sequestered to the inner portion of the cell wall. Through inhibition of LytG there is an increase in cell wall thickness and cross-linking, suggesting a reduction in the release of tension through the hydrolysis of the outermost layers of PG. Mas treatment also appears to be linked to DacA and D,D-transpeptidase activity. This reduction in hydrolysis prevents nascent PG from being pulled into the stress bearing layers of the cell wall, which in turn could impede the outward migration of LytE during growth. This would result in a sequestering of LytE to the inner face of the cell wall, manifesting in a dysregulation of the elongation complex with CwlO that would lead to the defects observed in the electron microscopy images.

Given that there is no change in total protein content, membrane permeability, or nucleic acid synthesis (Fig. S4) up to 2× the MIC of Mas, these observed alterations in the septal ring localization are not a consequence of alterations in macromolecular synthesis or membrane permeability. Increased levels of (p)ppGpp, as measured by *relA* transcript levels, result in a SigD "off" state, which has implications for cell chaining in *B. subtilis*[37] and is likely influencing the Mas-induced sausage-link-like phenotype and further impeding LytE outward migration. This is further supported by our previous observation that deletion of the SigD controlled autolysins LytD, LytC, and LytF result in increased sensitivity to Mas.[19] This ties into prior observations that PG hydrolases are required for controlling the stiffness of the Gram-positive cell wall.[11] Increased levels of (p)ppGpp and the corresponding decrease in GTP levels alleviates repression of the global transcriptional regulator CodY.[59] In addition to activating branched chain amino acid synthesis[59] CodY modulates clhAB2 operon which is involved in cell shape and regulating autolytic acitivity in *B. cereus*.[65] Based on our findings, we propose that inhibition of LytG by Mas initiates a cellular response of disregulated cell elongation and division through a reduction in turnover of the outer layers of PG and inability to release tension that results in the inability of LytE to migrate to the outer wall.

Conclusion

PG metabolism is a tightly coordinated, spatially separated system of biosynthetic and degradative processes. There are several reports of compounds that inhibit the activity of glycosidic autolysins (lytic transglycosylases, GlcNAcases) reported in the literature.[66–68] Mas is the first of these inhibitors to show inhibition of bacterial growth. The application of the small molecule inhibitor of the *exo*-GlcNAcase LytG, masarimycin, as a chemical probe to investigate the role of LytG has provided the first evidence for LytG involvement in the elongation and division complexes. A possible mechanism for this involves disruption of the migration of the essential endopeptidase LytE to the outer cell wall (Fig. 7). Inhibition of autolytic activity on the outer wall (*i.e.* LytG) releases tension allowing for newly synthesized PG inserted into the wall to be pulled into the stress bearing layer. This inhibition of tension release keeps LytE on the membrane side of the cell wall in complex with the elongation/division complex and the other essential endopeptidase CwlO resulting in disorganized elongation. This hypothesis is supported by previous observations that single knockouts in the autolysins LytD, LytC, and LytF act synergistically with Mas inhibition of LytG, suggesting involvement of these autolysins in releasing tension in the outer cell wall. This is further supported by the observation of thickened and rough cell wall in electron and atomic force microscopy.

Using both chemical biology and genetic approaches we have identified interactions between LytG activity and key players in cell wall elongation and division. Further, our combined approach highlights the difficulty in elucidating the mode-of-action of cell wall targeting molecules utilizing solely a genetic approach. This is highlighted by the demonstration that deletion of cell wall metabolism and division genes (*pbpA*, *minC*, *dacA*) impacts the levels of *exo*-GlcNAcase activity, likely contributing to the increased fitness observed in

genetic screens. These studies highlight the complex interactions between cell wall biosynthesis and degradation and the coordination with the elongation and division machinery. While these results do not completely elucidate the role of LytG in these processes, it does clearly identify several lines of inquiry for future studies.

Conflicts of interest

There are no conflicts to declare.

Data availability

Bacterial strains used in this article are available from the Bacillus Genetic Stock Center (**https://www.bgsc.org**). Data supporting this article have been included as part of the supplementary information (SI). Supplementary information is available. See DOI: **https://doi.org/10.1039/d5cb00151j**.

Acknowledgements

Research was supported by the National Science Foundation (CHE2401556). This project was supported in part by a grant from the National Center For Research Resources (NCRR) (1S 10RR021051) from the National Institutes of Health, Brown University's Division of Biology and Medicine and Provost's office.

References

1 J. Errington and L. T. V. Aart, *Microbiology*, 2020, **166**, 425–427.
2 W. Vollmer, D. Blanot and M. A. de Pedro, *FEMS Microbiol. Rev.*, 2008, **32**, 149–167.
3 A. P. Bhavsar and E. D. Brown, *Mol. Microbiol.*, 2006, **60**, 1077–1090.
4 M. Beeby, J. C. Gumbart, B. Roux and G. J. Jensen, *Mol. Microbiol.*, 2013, **88**, 664–672.
5 A. L. Koch and R. J. Doyle, *J. Theor. Biol.*, 1985, **117**, 137–157.
6 T. J. Silhavy, D. Kahne and S. Walker, *Cold Spring Harbor Perspect. Biol.*, 2010, **2**, a000414.
7 A. Gautam, R. Vyas and R. Tewari, *Crit. Rev. Biotechnol.*, 2011, **31**, 295–336.
8 P. Setlow, *Curr. Opin. Microbiol.*, 2003, **6**, 550–556.
9 W. Vollmer, *Mol. Microbiol.*, 2012, **86**, 1031–1035.
10 S. A. Blackman, T. J. Smith and S. J. Foster, *Microbiol*, 1998, **144**(Pt 1), 73–82.
11 R. Wheeler, R. D. Turner, R. G. Bailey, B. Salamaga, S. Mesnage, S. A. Mohamad, E. J. Hayhurst, M. Horsburgh, J. K. Hobbs and S. J. Foster, *mBio*, 2015, **6**, e00660.
12 G. Misra, E. R. Rojas, A. Gopinathan and K. C. Huang, *Biophys. J.*, 2013, **104**, 2342–2352.
13 A. Taguchi, D. Kahne and S. Walker, *Curr. Opin. Chem. Biol.*, 2019, **53**, 44–50.
14 M. A. Welsh, K. Schaefer, A. Taguchi, D. Kahne and S. Walker, *J. Am. Chem. Soc.*, 2019, **141**, 12994–12997.
15 F. A. Rubino, A. Mollo, S. Kumar, E. K. Butler, N. Ruiz, S. Walker and D. E. Kahne, *J. Am. Chem. Soc.*, 2020, **142**, 5482–5486.
16 M. Sjodt, K. Brock, G. Dobihal, P. D. A. Rohs, A. G. Green, T. A. Hopf, A. J. Meeske, V. Srisuknimit, D. Kahne, S. Walker, D. S. Marks, T. G. Bernhardt, D. Z. Rudner and A. C. Kruse, *Nature*, 2018, **556**, 118–121.
17 G. C. Lai, H. Cho and T. G. Bernhardt, *PLoS Genet.*, 2017, **13**, e1006934.
18 H. Kuhn, D. Gutelius, E. Black, C. Nadolny, A. Basu and C. Reid, *MedChemComm*, 2014, **5**, 1213–1217.
19 S. Nayyab, M. O'Connor, J. Brewster, J. Gravier, M. Jamieson, E. Magno, R. D. Miller, D. Phelan, K. Roohani, P. Williard, A. Basu and C. W. Reid, *ACS Infect. Dis.*, 2017, **3**, 421–427.
20 B. A. Haubrich, S. Nayyab, M. Gallati, J. Hernandez, C. Williams, A. Whitman, T. Zimmerman, Q. Li, Y. Chen, C.-Z. Zhou, A. Basu and C. W. Reid, *Microbiology*, 2022, 168.
21 G. J. Horsburgh, A. Atrih, M. P. Williamson and S. J. Foster, *Biochemistry*, 2003, **42**, 257–264.
22 M. Gallati, B. Point and C. W. Reid, *J. Vis. Exp.*, 2022, **179**, e63191.
23 J. C. Palomino, A. Martin, M. Camacho, H. Guerra, J. Swings and F. Portaels, *Antimicrob. Agents Chemother.*, 2002, **46**, 2720–2722.
24 M. A. Farha, T. L. Czarny, C. L. Myers, L. J. Worrall, S. French, D. G. Conrady, Y. Wang, E. Oldfield, N. C. Strynadka and E. D. Brown, *Proc. Natl. Acad. Sci. U. S. A.*, 2015, **112**, 11048–11053.
25 F. C. Odds, *J. Antimicrob. Chemother.*, 2003, **52**, 1.
26 A. P. d A. Pereira, P. A. M. d Andrade, D. Bini, A. Durrer, A. Robin, J. P. Bouillet, F. D. Andreote and E. J. B. N. Cardoso, *PLoS One*, 2017, **12**, e0180371.
27 R. E. Schaub and J. P. Dillard, *Bio-protocol*, 2017, **7**, e2438.
28 D. Kühner, M. Stahl, D. D. Demircioglu and U. Bertsche, *Sci. Rep.*, 2014, **4**, 7494.
29 P. Courtin, G. Miranda, A. Guillot, F. Wessner, C. Mezange, E. Domakova, S. Kulakauskas and M. P. Chapot-Chartier, *J. Bacteriol.*, 2006, **188**, 5293–5298.
30 E. Kuru, A. Radkov, X. Meng, A. Egan, L. Alvarez, A. Dowson, G. Booher, E. Breukink, D. I. Roper, F. Cava, W. Vollmer, Y. Brun and M. S. VanNieuwenhze, *ACS Chem. Biol.*, 2019, **14**, 2745–2756.
31 D. J. Novo, N. G. Perlmutter, R. H. Hunt and H. M. Shapiro, *Antimicrob. Agents Chemother.*, 2000, **44**, 827–834.
32 E. Kuru, H. V. Hughes, P. J. Brown, E. Hall, S. Tekkam, F. Cava, M. A. de Pedro, Y. V. Brun and M. S. VanNieuwenhze, *Angew. Chem., Int. Ed.*, 2012, 51, 12519–12523.
33 D. Morales Angeles, Y. Liu, A. M. Hartman, M. Borisova, A. de Sousa Borges, N. de Kok, K. Beilharz, J.-W. Veening, C. Mayer, A. K. H. Hirsch and D.-J. Scheffers, *Mol. Microbiol.*, 2017, **104**, 319–333.
34 D. L. Popham and P. Setlow, *J. Bacteriol.*, 1996, **178**, 2079–2085.
35 D. L. Popham and K. D. Young, *Curr. Opin. Microbiol.*, 2003, **6**, 594–599.

36 M. J. Tobin, S. Y. Cho, W. Profy, T. M. Ryan, D. H. Le, C. Lin, E. Z. Yip, J. L. Dorsey, B. R. Levy, J. D. Rhodes and M. A. Welsh, *Biochemistry*, 2023, **62**, 1342–1346.
37 Q. O. Ababneh and J. K. Herman, *J. Bacteriol.*, 2015, **197**, 128–137.
38 T. L. Czarny, A. L. Perri, S. French and E. D. Brown, *Antimicrob. Agents Chemother.*, 2014, **58**, 3261–3269.
39 T. M. Wendrich and M. A. Marahiel, *Mol. Microbiol.*, 1997, **26**, 65–79.
40 R. Chen, S. B. Guttenplan, K. M. Blair and D. B. Kearns, *J. Bacteriol.*, 2009, **191**, 5775–5784.
41 Y. Wei, T. Havasy, D. C. McPherson and D. L. Popham, *J. Bacteriol.*, 2003, **185**, 4717–4726.
42 M. Nakao, K. Yukishige, M. Kondo and A. Imada, *Antimicrob. Agents Chemother.*, 1986, **30**, 414–417.
43 M. F. Templin, D. H. Edwards and J. V. Höltje, *J. Biol. Chem.*, 1992, **267**, 20039–20043.
44 A. H. Williams, R. Wheeler, C. Thiriau, A. Haouz, M. K. Taha and I. G. Boneca, *Antibiotics*, 2017, **6**, 8.
45 P. S. Ocampo, V. Lázár, B. Papp, M. Arnoldini, P. A. Z. Wiesch, R. Busa-Fekete, G. Fekete, C. Pál, M. Ackermann and S. Bonhoeffer, *Antimicrob. Agents Chemother.*, 2014, **58**, 4573–4582.
46 P. J. Yeh, M. J. Hegreness, A. P. Aiden and R. Kishony, *Nat. Rev. Microbiol.*, 2009, **7**, 460–466.
47 S. Sharifzadeh, F. Dempwolff, D. B. Kearns and E. E. Carlson, *ACS Chem. Biol.*, 2020, **15**, 1242–1251.
48 P. J. Stogios and A. Savchenko, *Protein Sci.*, 2020, **29**, 654–669.
49 D. Rai, Jay K. Singh, N. Roy and D. Panda, *Biochem. J.*, 2008, **410**, 147–155.
50 D. Hwang and Y.-H. Lim, *Sci. Rep.*, 2015, **5**, 10029.
51 D.-J. Scheffers and J. Errington, *J. Bacteriol.*, 2004, **186**, 5153–5156.
52 R. López and E. García, *FEMS Microbiol. Rev.*, 2004, **28**, 553–580.
53 X. Wu, E. E. Paskaleva, K. K. Mehta, J. S. Dordick and R. S. Kane, *Sci. Rep.*, 2016, **6**, 35616.
54 M. Schlag, R. Biswas, B. Krismer, T. Kohler, S. Zoll, W. Yu, H. Schwarz, A. Peschel and F. Götz, *Mol. Microbiol.*, 2010, **75**, 864–873.
55 X. Wu, J. Han, G. Gong, M. A. G. Koffas and J. Zha, *FEMS Microbiol. Rev.*, 2020, 45.
56 H. G. Calamita and R. J. Doyle, *Mol. Microbiol.*, 2002, **44**, 601–606.
57 J. Wecke, M. Perego and W. Fischer, *Microb. Drug Resist.*, 1996, **2**, 123–129.
58 L. X. Chen, S. He, C. Li and J. Ryu, *J. Exp. Microbiol. Immunol*, 2009, **13**, 53–57.
59 A. O. Gaca, C. Colomer-Winter and J. A. Lemos, *J. Bacteriol.*, 2015, **197**, 1146–1156.
60 E. Cendrowicz, S. P. van Kessel, L. S. van Bezouwen, N. Kumar, E. J. Boekema and D. J. Scheffers, *PLoS One*, 2012, **7**, e43293.
61 M. Wenzel, I. N. Celik Gulsoy, Y. Gao, Z. Teng, J. Willemse, M. Middelkamp, M. G. M. van Rosmalen, P. W. B. Larsen, N. N. van der Wel, G. J. L. Wuite, W. H. Roos and L. W. Hamoen, *Proc. Natl. Acad. Sci. U. S. A.*, 2021, **118**, e2002635118.
62 J. A. Gregory, E. C. Becker and K. Pogliano, *Genes Dev.*, 2008, **22**, 3475–3488.
63 M. Hashimoto, S. Ooiwa and J. Sekiguchi, *J. Bacteriol.*, 2012, **194**, 4796–4803.
64 P. Dominguez-Cuevas, I. Porcelli, R. A. Daniel and J. Errington, *Mol. Microbiol.*, 2013, **89**, 1084–1098.
65 E. Huillet, L. Bridoux, P. Wanapaisan, A. Rejasse, Q. Peng, W. Panbangred and D. Lereclus, *PLoS One*, 2017, **9**, e0184975.
66 C. A. Clarke, E. M. Scheurwater and A. J. Clarke, *J. Biol. Chem.*, 2010, **285**, 14843–14847.
67 E. A. Martinez-Bond, B. M. Soriano and A. H. Williams, *Curr. Opin. Struct. Biol.*, 2022, **77**, 102480.
68 A. B. Mezoughi, C. M. Costanzo, G. M. Parker, E. M. Behiry, A. Scott, A. C. Wood, S. E. Adams, R. B. Sessions and E. J. Loveridge, *Molecules*, 2021, **26**, 4189.